JOURNAL OF MATERIALS SCIENCE 28 (1993) 4205–4211

Fabrication and characterization of $YBa_2Cu_3O_{7-x}$/Sn composite superconductors

Part I *Microstructure and mechanical properties*

R. CHAIM, Y. EZER
Department of Materials Engineering, Technion – Israel Institute of Technology, Haifa, 32000 Israel

$YBa_2Cu_3O_{7-x}$/Sn (YBCO/Sn) composites containing 15–50 wt% Sn were prepared by conventional powder metallurgy and pressureless liquid-phase sintering at 230 °C. Tin was found to wet YBCO, replace the porosity and distribute homogeneously among the YBCO grains. No reaction occurred between the two phases. Hardness changes were consistent with the observed microstructural features. Room-temperature compression tests revealed strains higher than 2% at the maximum stress, and stress–strain curves typical of composite cermets.

1. Introduction

The brittle behaviour of ceramic superconductors is one of the main disadvantages which restrict their engineering applications. This drawback may be overcome by incorporating a metallic phase within the bulk superconductor, so as to benefit from the properties of the composite material. However, the metallic component should be chemically, mechanically and electrically compatible with the ceramic substance. In this context, various techniques were used to fabricate composites of $YBa_2Cu_3O_{7-x}$ (YBCO) with noble metals such as silver [1–7] and gold [8, 9]. A few works were also published, involving more common metals such as tin [10, 11], aluminium and copper alloys [3, 12].

In order to achieve ductility in the composite cermet, it should contain some volume fraction of metal which, in turn, depends on the mutual wettability, and metrological parameters of the two phases. The high reactivity of YBCO led to investigations concerning its chemical compatibility with various substances [13–15]. It was shown that the superconducting transition temperature, T_c, may be preserved at a relatively high volume content (up to 10 mol %) of tin oxide [15]. In addition, tin was found to be adherent to YBCO [16].

The present work describes the microstructure and mechanical properties of the YBCO/Sn cermets fabricated by conventional powder metallurgy techniques. The Part II of this paper [17] will be concerned with the electrical properties of these composites.

2. Experimental procedure

$YBa_2Cu_3O_{7-x}$ was prepared in powder form by solid-state reaction of highly pure Y_2O_3, $BaCO_3$ and CuO powders, mixed in stoichiometric proportions. The mixture was fired in air at 950 °C for 24 h and then reground. This treatment was repeated twice, and the product (which revealed only reflections of orthorhombic $YBa_2Cu_3O_{7-x}$ in the X-ray diffraction spectrum) was mixed with appropriate proportions of the high-purity tin powders to give compositions of 15, 20, 25, 30, 35, 40 and 50 wt % Sn. The metal/ceramic powder mixtures were mechanically blended in an agate mortar for 0.5 h, followed by cold-die compaction under 200 MPa pressure. The pressed discs, 17 mm diameter and 5 mm thick, were then sintered at 230 °C for 1 h in air.

Specimens for optical and scanning electron (SEM, JSM-840) microscopy were prepared by dry sectioning and mechanical polishing of the composite specimens down to 0.25 μm, using water-free diamond slurry on nylon cloth. These specimens were used for Vickers hardness tests under a 0.3 kg load for a constant time of 10 s. The resulting indentations were large relative to the geometrical scale of the multiphase composites.

X-ray diffraction spectra were obtained for the as-sintered and as-cut surfaces, using a diffractometer (PW-1820) with CuK_α radiation, equipped with a graphite monochromator and operated at 40 kV and 40 mA. The scanning speed was 0.25 deg min^{-1}.

The compression tests were carried out on 4 mm × 4 mm × 4 mm cubes, at room temperature using an Instron machine (Model 1362) at a cross-head velocity of 50 μm min^{-1} (strain rate 10^{-4} s^{-1}). The top and bottom compressed surfaces of the cubes were sparingly lubricated with a silicone grease prior to the tests, in order to minimize the tangential frictional forces.

3. Results

Typical SEM images from the ground YBCO and the as-received tin powders are shown in Fig. 1. The

0022–2461

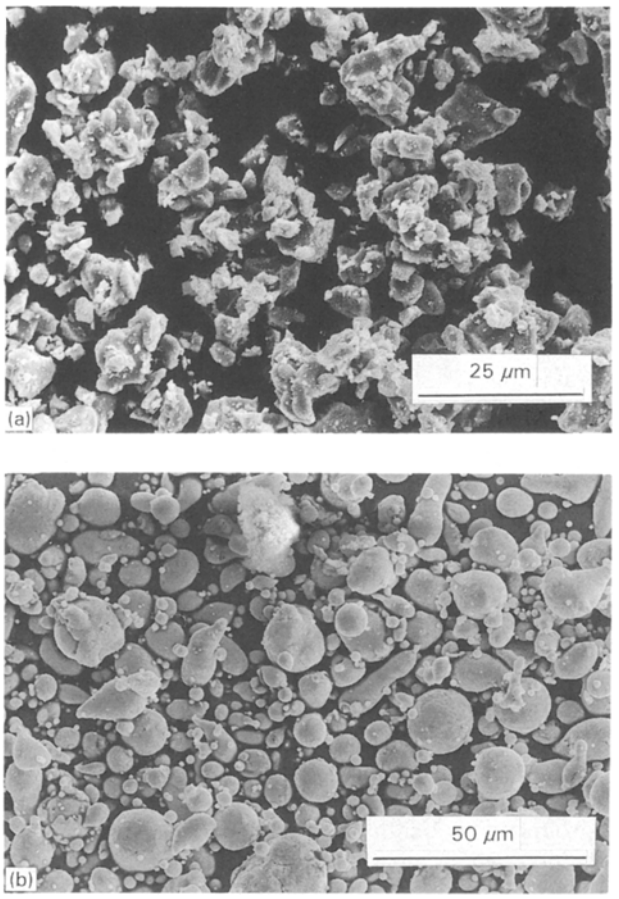

Figure 1 Scanning electron micrographs of (a) as-ground YBCO powder with irregular morphology, (b) as-received tin powder with spherical morphology.

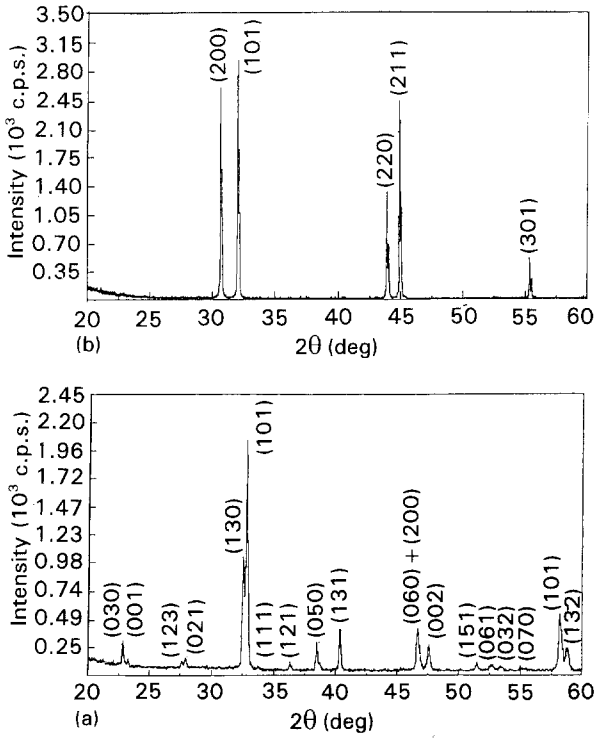

Figure 2 X-ray diffraction spectra of (a) as-ground YBCO, $x < 0.2$, powder with orthorhombic symmetry, (b) as-received tin (β-Sn) powder free of any reflections of tin oxides.

YBCO powder particles (Fig. 1a) were of irregular shape compared with the spherical morphology of the tin particles (Fig. 1b). Some agglomeration was also noted in the YBCO powder. The particle-size distribution of both powders fell within the 1–20 μm range. The green compacts were of sufficient strength for further handling.

X-ray diffraction spectra verified the orthorhombic symmetry of the YBCO powder (Fig. 2a). The tin powder was oxide-free (Fig. 2b).

Characteristic microstructures of the composite samples sintered at 230 °C are shown in Fig. 3a–e. The metallic phase consists mostly of isolated particles (bright), dispersed homogeneously among the ceramic grains (grey). The grain-size distribution of both the ceramic and metallic phases were similar to that of the original powders. The regions adjacent to the tin particles often appeared to be the densest. In addition, visual inspection revealed a systematic decrease in porosity as the tin content increased. The corrugated surfaces of the tin particles at the YBCO/Sn interfaces are evidence of their satisfactory wetting effect.

No reaction-product phases were detected at the YBCO/Sn interfaces, even at a very high SEM magnification (Fig. 4). Microchemical analyses by energy dispersive spectroscopy (EDS) likewise failed to detect traces of diffusive elements in adjacent grains of either tin or YBCO.

X-ray diffraction spectra from samples with different tin contents are shown in Fig. 5, the increase in tin being manifested in increase in the relative intensity of its diffraction peaks. The orthorhombic phase was preserved, and no new peaks were observed, indicating no reaction between the two phases. Very weak diffraction peaks from tin monoxide (SnO) were observed, corresponding to a few per cent (< 3 wt %) of this phase. These findings apply to all samples, irrespective of their tin content.

Quantitative density measurements showed a continuous decrease in true porosity as function of the tin content (Fig. 6), in agreement with the microstructural findings.

Results of the Vickers hardness tests as function of the tin content are shown in Fig. 7, each data point representing the average of ten indentations, and the standard deviation reflecting the homogeneity of the specimens.

Hardness is seen to decrease with increasing tin content. The indentation traces have sharp edges, without collapse of the surrounding grains.

Stress–strain curves based on the compression tests at room temperature are shown in Fig. 8. Several features may be noted in these curves. First, unlike the brittle-fracture behaviour of the pure YBCO ceramic, all the curves resemble patterns of plastic deformation, and although absolute values cannot be deduced, the increase in elastic modulus with tin content is evident. Secondly, there is a parallel significant improvement in toughness (proportional to the area below the curves); in this regard, the maximum compressive strength increases systematically with tin content, while the strain at maximum stress remains almost unchanged up to 40% Sn (Fig. 9).

Finally, all cermet specimens retained some residual strength after the maximum stress was reached. This

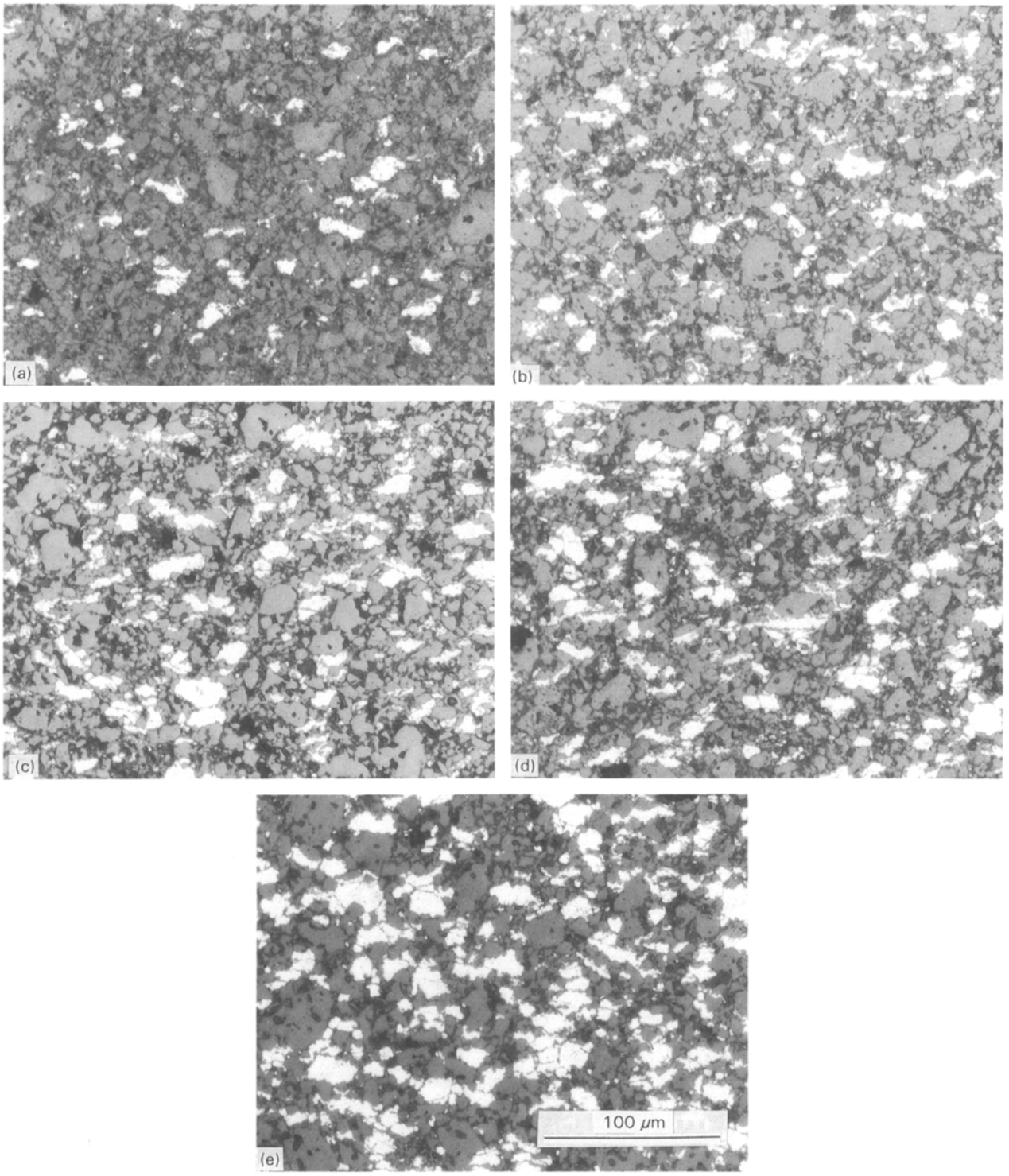

Figure 3 Optical micrographs of the $YBa_2Cu_3O_{7-x}$/Sn composites, with different tin contents, showing homogeneous distribution of tin (bright) among the ceramic grains (grey). The porosity (black) decreases with tin content: (a) 15 wt %, (b) 20 wt %, (c) 25 wt %, (d) 30 wt %, (e) 35 wt % Sn.

residual strength increases with tin content as shown in Fig. 10, and is a measure of the reinforcement effect in the composite material.

In order to verify this mechanical behaviour of the composite, some specimens were cyclically loaded–unloaded beyond the maximum stress, as shown in Fig. 11 for the YBCO/30% Sn specimen. The reversal of the curve on reloading, close to the unloading point, which indicates an apparent irreversible strain, is attributable to formation and propagation of internal microcracks (see also last paragraph in this section).

Fractography was performed in the SEM, and typical results are shown in Fig. 12. Fig. 12a shows the macroscopic view and a fracture of the YBCO–35% Sn compressed cube, composed of shear-type surfaces. Most of the composite specimens failed in a similar mode in the compression tests, irrespective of their tin content. At higher magnifications, these fractures reveal brittle fracture of the YBCO grains (Fig. 12b) as well as traces of plastic deformation in tin (Fig. 12c), most probably caused by sliding of the adjacent YBCO grains. This final piece of evidence may indi-

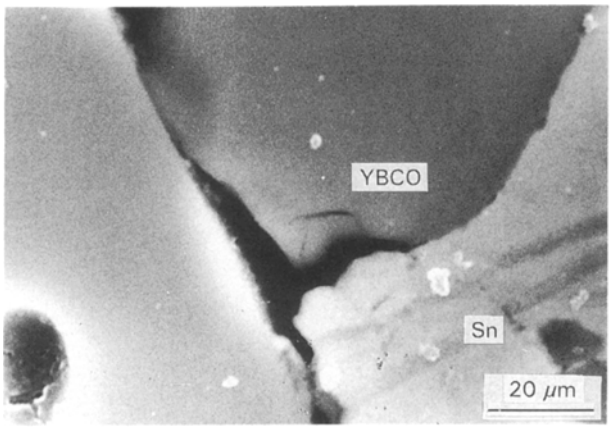

Figure 4 SEM image of the $YBa_2Cu_3O_{7-x}$/Sn interface at high magnification, demonstrating the satisfactory wetting of the YBCO surface by the tin. No detectable traces of diffusing elements were observed by EDS on either side.

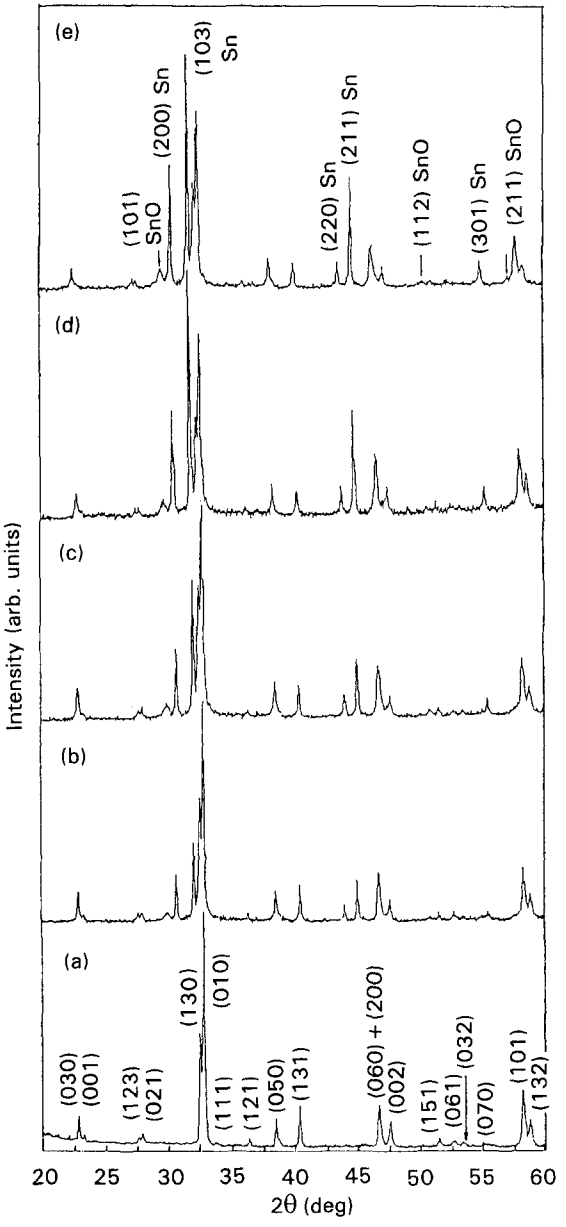

Figure 5 X-ray diffraction spectra of the $YBa_2Cu_3O_{7-x}$/Sn composites with different tin contents, demonstrating the absence of reaction. Some oxidation of tin during sintering was indicated by the presence of tin oxide reflections: (a) 0 wt%, (b) 15 wt%, (c) 20 wt%, (d) 25 wt%, (e) 30 wt% Sn.

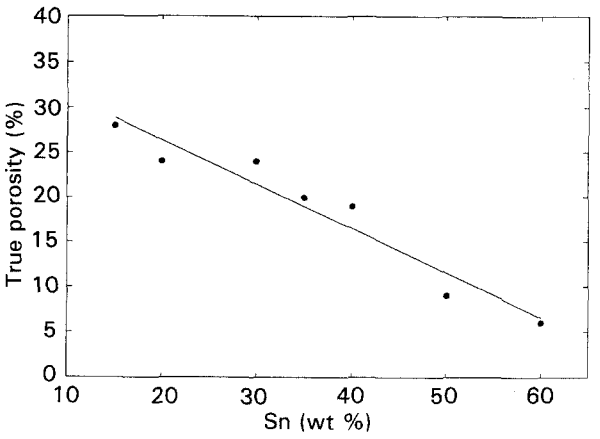

Figure 6 Systematic decrease of the true porosity with tin content in $YBa_2Cu_3O_{7-x}$/Sn composites sintered at 230 °C for 1 h in air.

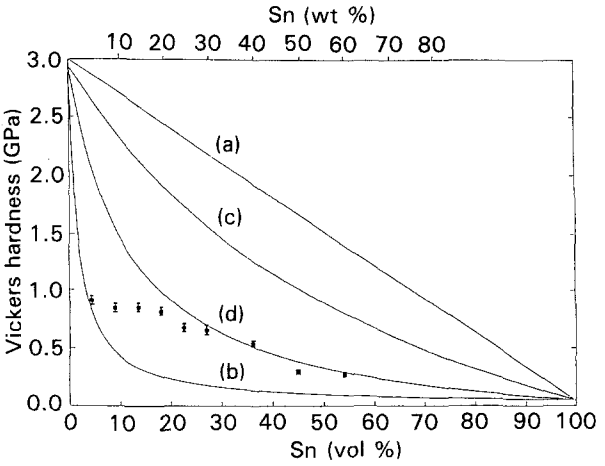

Figure 7 (○) Experimental and (——) calculated hardness values for different compositions of the YBCO/Sn composites, using the (a) Voigt, (b) Reuss, and (c, d) Hashin–Shtrikman models. See text for further discussion.

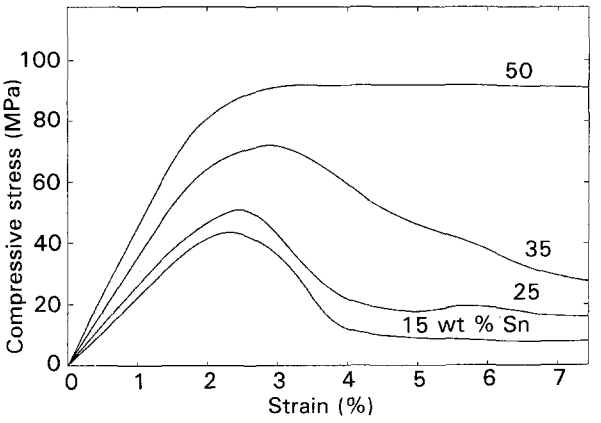

Figure 8 Characteristic compressive stress–strain curves of the YBCO/Sn composites. Increase in the elastic moduli and maximum stress with tin content was observed.

cate relatively strong bonding at the ceramic/metal interfaces.

In addition, arrays of microcracks aligned perpendicular to the shear directions were found to coalesce as shown in Fig. 12d. These microcracks, which most probably nucleate at the original porosities, contribute to the apparent irreversible strain, in addition to the true plastic deformation and sliding in tin.

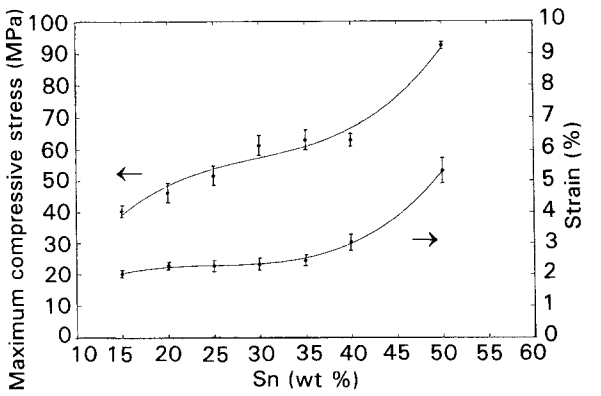

Figure 9 Maximum compressive stress and its corresponding strain versus tin content in the YBCO/Sn composites.

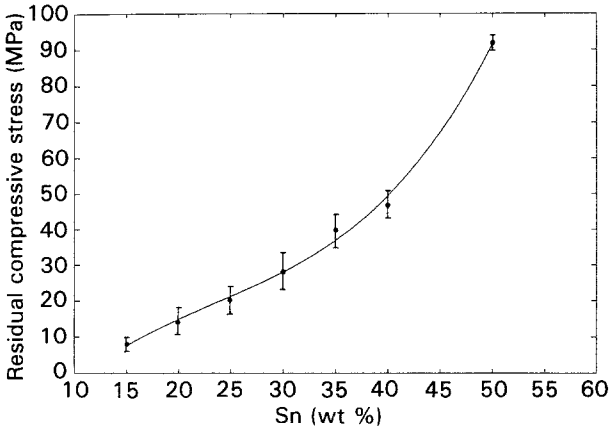

Figure 10 Residual compressive strength at 5% strain (beyond the maximum stress) was determined as a measure for the reinforcement effect as function of tin content.

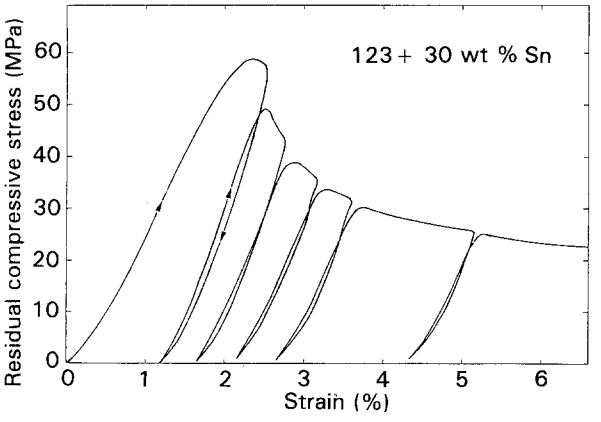

Figure 11 Loading–unloading cycles (beyond the maximum stress) in the YBCO–30 wt % Sn specimen, exhibiting the "memory effect" typical of composites.

4. Discussion

The fact that the green compacts have relatively good structural integrity even at the lowest tin contents, indicates that YBCO particles were "welded" by the tin grains in a continuous manner. This effect was undoubtedly facilitated by the mechanical mixing of the two original powders, during which tin grains were smeared on the YBCO grain surfaces.

The absence of chemical reaction at 230 °C is a consequence of the relatively low diffusion coefficient of tin in YBCO at this temperature ($\sim 10^{-11}$ cm^2 s^{-1}, [18]). However, on the basis of the observed microstructure, the porosities are replaced by tin during the warm-temperature sintering, as a result of flow of the liquid tin into them (this is also consistent with the decrease in porosity with increasing tin content, in the absence of sintering shrinkage as a porosity-reducing factor). However, the low depth of diffusion (~ 2 μm) suffices for chemical bonding between the two phases.

For the hardness and its variation with tin content, we assumed that due to the hydrostatic pressure below the indentor, the bulk modulus, K, would be the best parameter on which the average hardness, H, of the composite may be modelled. Accordingly, the maximal and minimal hardness values of the two-phase composite were calculated, using the Voigt and Reuss models for composites with parallel phases

$$H_{max} = V_1 H_1 + V_2 H_2 \quad \text{(Voigt)} \quad (1)$$

$$1/H_{min} = V_1/H_1 - V_2/H_2 \quad \text{(Reuss)} \quad (2)$$

and the modified Hashin–Shtrikman model [19] for randomly distributed phases, for the present cermets, where $K_1 = 0.22G_1$ (for tin [20]) and $K_2 = 2G_2$ (for YBCO [21])

$$H_{max} = H_2 + V_1/[(1/H_1 - H_2) + (3V_2/5H_2)] \quad (3)$$

$$H_{min} = H_1 + V_2/[(1/H_2 - H_1) + (V_1/7H_1)] \quad (4)$$

where G is the shear modulus, V_i the volume fraction of the i phase, and the subscripts 1 and 2 refer to tin and YBCO, respectively.

The calculated hardness values are shown in Fig. 7. The fit of the experimental data with the lower bound of the Hashin–Shtrikman model, which represents the exact solution for the spherical second-phase particles, is in agreement with the round-shape morphology of the tin particles.

Comparison of our data with those of Goyal *et al.* [10] shows higher hardness values (over 60%) in the present work, especially for low tin compositions. Although no decrease in hardness was observed at low tin contents, extrapolation to zero tin content indicated a rapid drop in hardness due to the unsintered nature of these compacts, a drop actually reported by Goyal *et al.* at $\sim$ 20 wt % Sn. This effect is attributable to the high volume fraction of the porosity associated with a low tin content, and independent of the electrical percolation in the composite (see Fig. 2 in Part II [17]). On the other hand, the composition at which this drop is expected depends upon the metrological parameters of the phases, and on the porosity characteristics of the composite. The increase in elastic moduli (Fig. 8) with the tin content clearly demonstrates the role of the porosity in reducing the mechanical response of these cermets.

Room-temperature deformation of YBCO specimens under hydrostatic pressure and strain rate 10^{-4} s^{-1} [22], confirmed the brittle behaviour of this material. At the same time, reinforcement of YBCO by a metallic phase such as silver [23, 24] was shown to

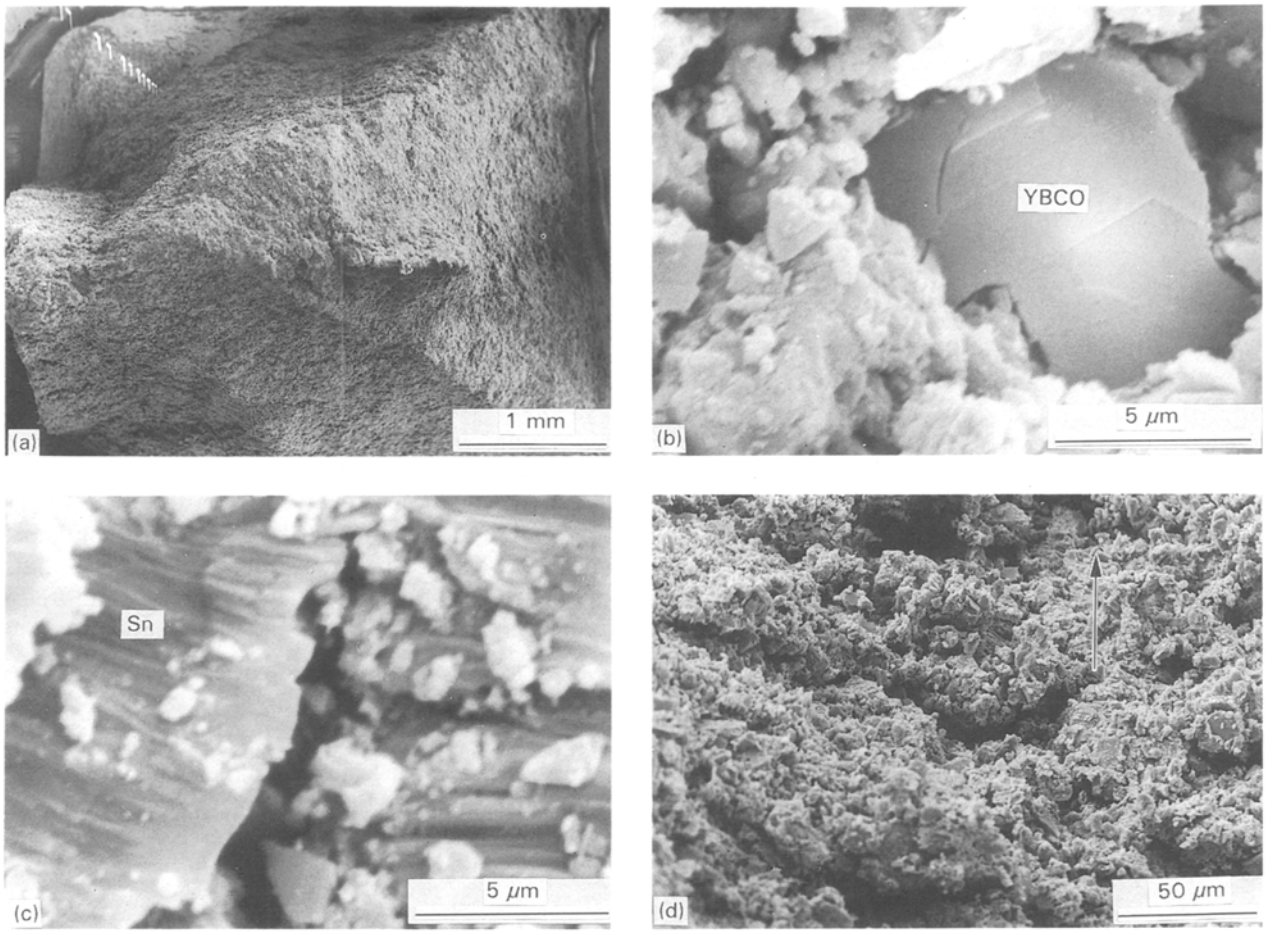

Figure 12 SEM fractographs of the YBCO–35% Sn composite. (a) Low-magnification image shows the macroscopic shear surfaces at an angle to the compression direction (perpendicular to the micrograph). (b) Brittle fracture of YBCO, and (c) ductile fracture of tin. (d) Coalescence of the microcracks perpendicular to the shear direction (arrow).

be feasible, resulting in strong bonding at the ceramic/metal interfaces. The microstructural observations and fractography of the present specimens confirmed wetting of YBCO by tin and revealed good bonding at their interfaces. Consequently, cracks form at stress concentrators such as the residual porosities as well as at twin kinks [25]. Still, the deformation is irreversible due to the presence of the metallic ductile phase. These characteristics are then responsible for the shape of the stress–strain curves, which are typical of composite cermets.

Finally, as could be seen from the deformation tests, strains above 2% were easily achieved at the maximum stress. Compared with the typical strain values of 0.1%–0.5% measured for pure YBCO [26], this indicates significantly higher ductility of the YBCO/Sn cermets. Compression tests up to the melting point of tin are under way to check the feasibility for crack-free hot-working.

Acknowledgements

The authors thank the Sachs Centre, Department of Materials Engineering, for providing the facilities used for this study. Partial financial support by the Fund for the Promotion of Research at the Technion is also acknowledged.

References

1. J. J. LIN and T.-M. CHEN, *Z. Phys. B* **81** (1990) 13.
2. H. K. VARMA, K. P. KUMAR, K. G. K. WARRIER and A. D. DAMODARAN, *Supercond. Sci. Technol.* **3** (1990) 73.
3. L. E. MURR and C. S. NIOU, *ibid.* **3** (1990) 173.
4. A. MATSUMURO, K. KASUMI, U. MIZUTANI and M. SENOO, *J. Mater. Sci.* **26** (1991) 737.
5. W. GAO, S.-C. LI, R. PARRELLA, D. A. RUDMAN and J. B. VANDER SANDE, *ibid.* **26** (1991) 4186.
6. P. A. CURRERI, P. N. PETERS, R. C. SISK, M. K. WU and C. Y. HUANG, *Met. Trans.* **21A** (1990) 257.
7. H. R. KHAN, T. L. FRANCAVILLA, R. A. HEIN, C. S. PANDE, S. B. QADRI, R. J. SOULEN, Jr., and S. A. WOLF, *J. Supercond.* **3** (1990) 189.
8. F. H. STREITZ, M. Z. CIEPLAK, G. XIAO, A. BAKHSHAI and C. L. CHIEN, *Appl. Phys. Lett.* **52** (1988) 927.
9. R. D. RAY II and E. E. HELLSTROM, *J. Appl. Phys.* **66** (1989) 741.
10. A. GOYAL, P. D. FUNKENBUSCH, G. C. S. CHANG and S. J. BURNS, in "Superconductivity and its Applications", edited by H. S. Kwok and D. T. Show (Elsevier Science, Buffalo, NY, 1988) p. 223.
11. C. T. HO and D. D. CHUNG, *J. Mater. Res.* **4** (1989) 1339.
12. I.-G. CHEN, S. SEN and D. M. STEFANESCU, *Appl. Phys. Lett.* **52** (1988) 1355.
13. T. SUZUKI, T. YAMAZAKI, A. KOUKITSU, H. SEKI and K. TAKAHASHI, *J. Mater. Sci. Lett.* **8** (1989) 19.
14. T. SUZUKI, T. YAMAZAKI, R. SEKINE, A. KOUKITU, H. SEKI and K. TAKAHASHI, *ibid.* **8** (1989) 1271.
15. T. SUZUKI, T. YAMAZAKI, A. KOUKITU, M. MAEDA, H. SEKI and K. TAKAHASHI, *ibid.* **7** (1988) 926.
16. C. S. PANDE, H. A. HOFF, A. K. SINGH, M. S. OSOF-

SKY, M. A. IMAM, K. SADANANDA and L. E. RICHARDS, *IEEE Trans. Magn.* **25** (1989) 2004.
17. R. CHAIM and Y. EZER, *J. Mater. Sci.* in press.
18. V. N. ALFEEV, P. P. GORBIK, V. V. DYAKIN, F. A. ZAITOV, V. M. OGENKO and G. M. SHALYAPINA, *Solid State Commun.* **77** (1991) 49.
19. Z. HASHIN and S. SHTRIKMAN, *J. Mech. Phys. Solids* **11** (1963) 127
20. T. LYMAN (ed.), "Metals Handbook", 8th Edn, Vol. 1, "Properties and Selection of Metals" (ASM, Metals Park, OH, 1961) p. 1142.
21. H. LEDBETTER and M. LEI, *J. Mater. Res.* **6** (1991) 2253.
22. M. J. KRAMER, L. S. CHUMBLEY and R. W. McCALLUM, *J. Mater. Sci.* **25** (1990) 1978.
23. S. SAMAJDAR, A. KUMAR, K. MALLICK and S. K. SAMANTA, *J. Mater. Sci. Lett.* **9** (1990) 137.
24. H. K. VARMA, K. G. K. WARRIER and A. D. DAMODARAN, *ibid.* **9** (1990) 1000.
25. J. P. ZHOU, S. X. DOU, A. J. BOURDILLON, H. K. LIU and C. C. SORRELL, *ibid.* **8** (1989) 1147.
26. K. SALAMA, K. RAVI-CHANDAR, V. SELVAMANICKAM, D. F. LEE, P. K. REDDY and S. V. RELE, *J. Mineral. Met. Mater. Soc.* **40** (1988) 6.

Received 12 October 1992
and accepted 11 January 1993